Editors' Suggestion

Anomalous Hall Effect due to Magnetic Fluctuations in a Ferromagnetic Weyl Semimetal

Ola Kenji Forslund,[1,2,*] Xiaoxiong Liu,[3] Soohyeon Shin,[4] Chun Lin,[1] Masafumi Horio,[1] Qisi Wang,[1,5] Kevin Kramer,[1] Saumya Mukherjee,[6] Timur Kim,[6] Cephise Cacho,[6] Chennan Wang,[7] Tian Shang,[8] Victor Ukleev,[9,10] Jonathan S. White,[9] Pascal Puphal,[4,11] Yasmine Sassa,[12] Ekaterina Pomjakushina,[4] Titus Neupert,[1] and Johan Chang[1]

[1]*Physik-Institut, Universität Zürich, Winterthurerstrasse 190, CH-8057 Zürich, Switzerland*
[2]*Department of Physics and Astronomy, Uppsala University, Box 516, SE-75120 Uppsala, Sweden*
[3]*Department of Physics, Southern University of Science and Technology (SUSTech), Shenzhen 518055, China*
[4]*Laboratory for Multiscale Materials Experiments, PSI Center for Neutron and Muon Sciences, Forschungsstrasse 111, 5232 Villigen PSI, Switzerland*
[5]*Department of Physics, The Chinese University of Hong Kong, Shatin, Hong Kong, China*
[6]*Diamond Light Source, Didcot OX11 0DE, United Kingdom*
[7]*Paul Scherrer Institute, Laboratory for Muon Spin Spectroscopy, CH-5232 PSI Villigen, Switzerland*
[8]*Key Laboratory of Polar Materials and Devices (MOE), School of Physics and Electronic Science, East China Normal University, Shanghai 200241, China*
[9]*Laboratory for Neutron Scattering and Imaging (LNS), PSI Center for Neutron and Muon Sciences, Forschungsstrasse 111, 5232 Villigen PSI, Switzerland*
[10]*Helmholtz-Zentrum Berlin für Materialien und Energie, Berlin, Germany*
[11]*Max-Planck-Institute for Solid State Research, Heisenbergstraße 1, 70569 Stuttgart, Germany*
[12]*Department of Applied Physics, KTH Royal Institute of Technology, SE-106 91 Stockholm, Sweden*

(Received 1 September 2024; revised 6 December 2024; accepted 13 February 2025; published 24 March 2025)

The anomalous Hall effect (AHE) has emerged as a key indicator of time-reversal symmetry breaking (TRSB) and topological features in electronic band structures. Absent of a magnetic field, the AHE requires spontaneous TRSB but has proven hard to probe due to averaging over domains. The anomalous component of the Hall effect is thus frequently derived from extrapolating the magnetic field dependence of the Hall response. We show that discerning whether the AHE is an intrinsic property of the field-free system becomes intricate in the presence of strong magnetic fluctuations. As a study case, we use the Weyl semimetal PrAlGe, where TRSB can be toggled via a ferromagnetic transition, providing a transparent view of the AHE's topological origin. Through a combination of thermodynamic, transport, and muon spin relaxation measurements, we contrast the behavior below the ferromagnetic transition temperature to that of strong magnetic fluctuations above. Our results on PrAlGe provide general insights into the interpretation of anomalous Hall signals in systems where TRSB is debated, such as families of kagome metals or certain transition metal dichalcogenides.

DOI: 10.1103/PhysRevLett.134.126602

Intrinsic anomalous Hall effect (AHE) [1,2], characterized by transverse Hall conductance in the absence of an external magnetic field, has garnered significant attention as a probe of time-reversal symmetry breaking (TRSB) and topological features in electronic systems [3–6]. Unlike extrinsic AHE, which is driven by asymmetric scattering processes, intrinsic AHE (from here on AHE) is rooted in the nonzero integral of the Berry curvature [7]. Understanding the microscopic origins behind an observed Hall signal is vital, as spontaneous TRSB is a prerequisite for AHE. However, despite these profound implications, detecting and analyzing AHE is challenging due to magnetic domain formation. Therefore, externally applied magnetic fields are commonly utilized to lift the domain degeneracy. The AHE is in this case derived from extrapolating observed Hall resistance to the zero field (ZF) limit [7].

In ferromagnetic Weyl semimetals, the intrinsic anomalous Hall conductivity for small magnetic fields ($\boldsymbol{B}$) is proportional to $\boldsymbol{B}$, the sum of externally applied field ($\boldsymbol{H}$) and magnetization ($\boldsymbol{M}$) (other Weyl semimetals exist in which the average magnetization is not the suitable TRSB order parameter to serve as a proxy for the AHE [8]). Therefore, $\boldsymbol{H}$ and

*Contact author: ola.forslund@physik.uzh.ch

temperature (T) dependence of $\boldsymbol{B}$ serve as a estimate for the expected anomalous Hall conductivity. This indirect approach can, however, obscure whether the observed AHE is intrinsic or induced by the applied magnetic field. Differentiating these two scenarios is difficult and hence complicating the interpretation of many experiments [9–14].

The case of PrAlGe, a ferromagnetic (FM) Weyl semimetal, offers a unique opportunity to disentangle these effects. PrAlGe is a well-characterized topological ferromagnet ($T_C = 15$ K) stabilized in a noncentrosymmetric structure (space group $I4_1md$, no. 109). Because of broken inversion symmetry, Weyl points are expected to persist at all temperatures [15]. By utilizing temperature as a control parameter, we can precisely navigate between the ferromagnetic state (with TRSB) and the paramagnetic state (without TRSB), allowing us to systematically explore the AHE's dependence on magnetic order, effectively distinguishing between intrinsic and external contributions.

In this Letter, we report a Hall resistance study across the ferromagnetic transition. Consistent with previous reports, an intrinsic Hall effect is observed in the ordered state, which is derived from ZF extrapolation. We demonstrate that a similar extrapolated response is found in the paramagnetic phase. Muon spin relaxation (μ^+SR) measurements reveal the absence of short-range magnetic order or domain formations, ruling out TRSB above the ferromagnetic ordering temperature. In the presence of short-range magnetic order or domain formations, μ^+SR spectra typically exhibit either a sum of highly relaxing Gaussian-like functions or a combination of exponential terms. However, our μ^+SR results do not show these features and the data are consistent with the presence of dynamic paramagnetic fluctuations. Instead, we show that the application of a magnetic field in the presence of strong ferromagnetic fluctuations can induce a finite magnetization, as an immediate consequence of the proximate mean-field transition. This, in turn, produces a finite ZF extrapolated Hall effect. We therefore demonstrate that an extrapolated AHE is not a definitive indicator of TRSB. As such, our Letter establishes a framework for accurately interpreting the anomalous Hall measurements.

Single-crystalline PrAlGe [based on Pr (99.9%, pieces, ChemPur), Ge (99.999%, pieces, Alfa Aesar), and Al (99.99%, granules, ChemPur)] were grown using both the Al-flux method and floating-zone methods as described in Refs. [16,17]. Flux-grown single crystals were used for the electrical and magnetic susceptibility measurements, whereas the floating-zone crystals were used for angle resolved photo emission spectroscopy (ARPES) measurements. Polycrystalline samples for the μ^+SR measurements were prepared by arc melting, as described in Ref. [18]. All samples were characterized through x-ray diffraction, resistivity, and dc magnetization, confirming their quality and consistent ferromagnetic transition temperature of $T_C \simeq 15$ K, ensuring comparable magnetic properties [19]. The experimental setup of each technique is described in the End Matter and summarized in Table I.

To confirm the electronic band structure below and above T_C, we carried out ARPES. Previous density functional theory calculations [15] predicted Weyl points near the zone center. A photon energy ($h\nu$) scan determines that $h\nu = 34$ and 28 eV cuts through the zone center and boundary, respectively [see Fig. 4(c)]. Figures 1(a) and 1(b) show the measured Fermi surface (FS) collected using $h\nu = 34$ eV photons for temperatures below and above T_C, as indicated. The observed FS is consistent with a previously reported study conducted at $T \sim 11$ K [20], that, however, did not address the paramagnetic state ($T > T_C$). U-shaped contours, present at the Fermi level, were interpreted as Fermi arcs. We find that the reported Fermi arcs are also present at $T = 25$ K [Fig. 1(b)], which confirms the existence of Weyl points even in the paramagnetic phase.

A vertical momentum cut (cut 1, parallel to $\Gamma - M$) at $k_1 \simeq -0.18$ Å^{-1} passes through a pair of "U" states and two bands approaching the Fermi level are observed [Figs. 1(c) and 1(e)]. Based on the predicted location of the Weyl nodes, one of these linear bands was previously interpreted as left- and right-moving chiral edge modes [20]. This is further enhanced in their respective momentum distribution curves for selected binding energies [Figs. 1(d) and 1(f)]. Given the lack of any significant temperature dependence in the band structure, these Weyl points are most likely originating from the inversion symmetry breaking rather than TRSB from the FM order. The difference in intensity between the two temperatures is attributed to surface aging.

To characterize the magnetic properties of PrAlGe, temperature-dependent inverse magnetic susceptibility (χ) is shown in Fig. 2(a). A Curie-Weiss (CW) behavior is observed for $T > 80$ K and the positive value of the Weiss constant suggests FM interactions, consistent with previous reports [19,21]. Deviation from linearity is observed below

TABLE I. Summary of samples used in each experiment. For reference, previous experimental studies cited in this Letter, which are based on different growth methods, are listed as well.

Growth method	Crystal form	Experimental techniques	T_C [K]	Refs.
Al flux	Single crystal	Hall effect, magnetic susceptibility	15	[17,19–21]
Floating zone	Single crystal	ARPES	15	[17,19]
Arc melting	Polycrystal	μ^+SR	15	[17,18]

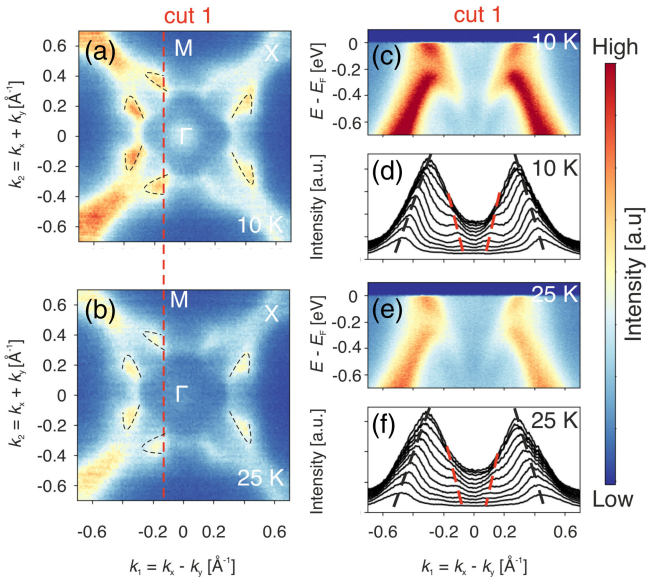

FIG. 1. (a), (b) ARPES intensity recorded at the Fermi level with $h\nu = 34$ eV photons for temperatures as indicated. The dashed black lines corresponds to the U-shaped Fermi arcs reported in Ref. [20]. (c), (e) Band dispersion through the U-shaped Fermi arc (cut 1) for $T = 10$ and 25 K, respectively. (d), (f) Momentum distribution curves from (c), (e) at selected binding energies. The dashed lines are guides to the eye.

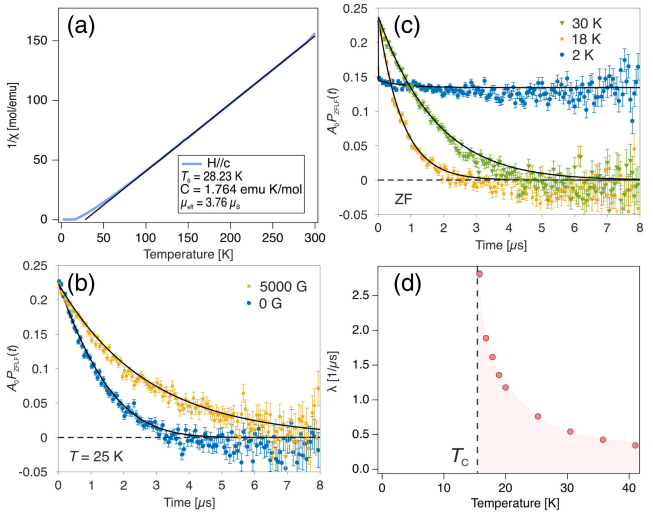

FIG. 2. (a) Inverse magnetic susceptibility (χ) as a function of temperature. The solid line is a linear fit based on Curie-Weiss law. Fit parameters are shown in the figure inset. (b) ZF and LF muon time spectra collected at $T = 25$ K. Solid lines are fits described in the main text and Appendix D. (c) ZF muon time spectra for selected temperatures. The solid lines, above T_C, are fits to extract the muon spin relaxation rate (λ)—see main text and Appendix D. (d) Temperature dependence of λ above T_C. The colored area is a guide to the eye. The vertical dashed lines indicate the critical temperature $T_C = 15$ K.

80 K, well above the FM ordering temperature $T_C = 15$ K. This FM state is stabilized via spin polarized f-electron states aligned along the FM easy axis (c axis) [19]. Deviations from the CW law may signal a gradual slowing down of dynamic spin-spin correlations due to thermal fluctuations. This involves a relatively large magnetic interaction strength, $J \sim k_B T$, likely dominated by interactions along the c axis [19], where spins interact and fluctuate coherently over short timescales. These anisotropic spin interactions along the c axis contribute to enhanced spin fluctuations across a broad temperature range [22]. As the system approaches T_C, these fluctuations become slower, leading to the development of effective internal magnetic fields, which facilitates an induced magnetization under an external magnetic field.

To confirm the outlined scenario, we measured ZF μ^+SR time spectra as a function of temperature [Fig. 2(c)]. μ^+SR is a sensitive magnetic probe for detecting both static and dynamic local magnetic fields in the megahertz to gigahertz range. The ZF time spectra display an exponential depolarization. Using the fit function $A_0 P_{\mathrm{ZFLF}}(t) = A G^{\mathrm{LFSGKT}}(\Delta, t, B_{\mathrm{LF}}) e^{-\lambda t}$, with $G^{\mathrm{LFSGKT}}(\Delta, t, B_{\mathrm{LF}})$ being the longitudinal field static Gaussian Kubo-Toyabe function [23], we find a relaxation rate of $\lambda \simeq 0.7$ μs^{-1} (the fit function is further explained and justified in Appendix D). In ZF, $B_{\mathrm{LF}} = 0$ and G^{LFSGKT} reduces into G^{SGKT}. As $G^{\mathrm{SGKT}}(\Delta, t)$ represents the depolarization originating from nuclear magnetic moments (mostly $I^{27}_{\mathrm{AL}} = 5/2$ and $I^{131}_{\mathrm{Pr}} = 5/2$), it is expected to be independent of temperature and a value of $\Delta = 0.15$ μs^{-1} was obtained (see Appendix D). This implies that any temperature dependence originates from the $e^{-\lambda t}$ term. This term represents the depolarization originating from electronic moments and its temperature dependence is presented in Fig. 2(d). The relaxation rate (λ) exhibits the maximum value close to T_C and gradually decreases with increasing temperature. Since the relaxation rate is inversely proportional to the spin-spin correlation frequency [23], the increase close to T_C is understood as a critical slowing down of fluctuating electronic moments close to T_C and is in line with the described scenario based on the magnetization measurements. This kind of increase close to T_C is commonly observed in many second order magnetic transitions [24–26].

The exponential relaxation in the time spectra [Figs. 2(b) and 2(c)] suggests a dynamic state. However, even static field distribution may in certain cases yield exponential-like relaxation if the internal field distribution is Lorentzian rather than Gaussian. Here, we confirm the dynamic origin via a longitudinal field (LF) measurement [Fig. 2(b)]. If the internal field is static, application of weak LF should decouple the spectra (i.e., suppress the depolarization so that effectively $\lambda \simeq 0$ μs^{-1}). However, even a strong LF = 5000 G does not decouple the spectra and the internal field is confirmed to be dynamic (see Appendix D). This is in line with temperature-dependent resistivity study,

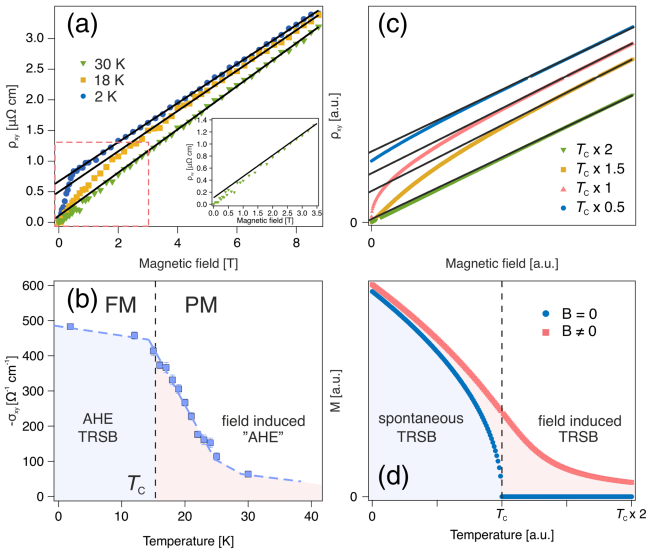

FIG. 3. (a) Hall resistivity (ρ_{xy}) as a function of magnetic field for temperatures as indicated. Solid lines are linear fits in the magnetic field range $H > 2.5$ T. Inset: the low magnetic field range as indicated by the dashed red rectangle in the main figure. (b) Temperature dependence of $\sigma_{xy}(H \to 0)$, obtained from linear fits in (a)—described in the main text. Below the critical temperature (T_C), spontaneous TRSB asserts the measured σ_{xy} to be anomalous Hall conductivity. Above T_C, the TRS is preserved and the measured σ_{xy} is instead an artifact from the applied magnetic field. The colored dashed line is a guide to the eye. (c) The calculated Hall resistivity curves as a function of magnetic field for selected temperature as indicated. (d) Calculated magnetization as a function of temperature for zero and finite magnetic fields. The calculations are explained in the main text and Supplemental Material [27].

in which measurements across T_C exhibit a sharp drop [19]. This drop is consistent with suppressed scattering from magnetic fluctuations in the FM phase, fluctuations that were prevailing in the paramagnetic state. It is also noted that previous neutron [19] and μ^+SR [18] measurements suggested the formation of nanosized magnetic domain wall spin textures in the FM phase. We may, however, conclude from our data that similar magnetic domains or smaller patches of long-range magnetic order can be excluded above T_C. This statement is based on the fact that Gaussian-like relaxation or oscillations are absent in the time spectra.

Having established both macroscopically and microscopically the existence of spin fluctuations above T_C, we next present temperature-dependent study of the AHE. The temperature dependence is determined from transverse resistivity (ρ_{xy}) isotherms, where a linear behavior is observed at higher fields [Fig. 3(a); see Figs. 4(a) and 4(b) for more temperatures]. This linear behavior is present even for temperatures above $T_C = 15$ K. The Hall resistivity in FM materials contains contributions from the ordinary (ρ^O_{xy}) and anomalous Hall resistivity (ρ^A_{xy}), where the intercept at ZF of the linear behavior extrapolated from higher fields defines ρ^A_{xy} [7]. The transverse conductivity can be evaluated based on ρ^A_{xy} via $\sigma_{xy} = -\rho^A_{xy}/(\rho^2_{xx} + \rho^2_{xy})$ and the temperature dependence is shown in Fig. 3(b).

The anomalous Hall conductivity saturates to $\sigma_{xy} \simeq 500\ \Omega^{-1}\,\mathrm{cm}^{-1}$ at 2 K, consistent with previous studies [10,19–21]. This value is close to the expected value from intrinsic Berry curvature contribution $\sigma_{xy} = (2\pi e^2/\hbar a) \simeq 600\ \Omega^{-1}\,\mathrm{cm}^{-1}$, where $\hbar$ is the reduced Planck's constant, e is the electric charge, and a is the lattice constant. While a conventional FM order is expected to give rise to a finite σ_{xy} due to extrinsic effects such as skew scattering or side jump, the amplitude is around 0.1–0.001 times of $(2\pi e^2/\hbar a)$ ($\sim$0.6–60 $\Omega^{-1}\,\mathrm{cm}^{-1}$) in PrAlGe [21], which is much smaller than observed [Fig. 3(b)]. Most importantly, however, large finite values of σ_{xy} are observed above T_C, up to 30 K. These kinds of observations have in the past been used to assert TRSB and AHE in different kinds of systems. We shall, however, show below that the observed behavior in this case can be ascribed to a magnetic field induced effect.

The large intrinsic anomalous Hall conductivity is explained within the framework of Berry curvature and finite Chern number. A prerequisite is a nonzero sum of Berry curvature, which in turn relies on TRSB. In PrAlGe, the inversion symmetry is broken by the lattice symmetry and the time-reversal symmetry is broken below $T_C = 15$ K, which is expected to shift the Weyl points in k space. This leads to a finite k range where the sum of Berry curvature becomes nonzero (due to the Zeeman coupling between the localized f electrons and the Weyl points), thereby realizing large intrinsic anomalous Hall conductivity in the FM phase (see Supplemental Material [27]) [15,30].

Above T_C, on the other hand, the time-reversal symmetry (TRS) is preserved as confirmed by μ^+SR. Yet, ZF extrapolated Hall conductivity is unequivocally measured [Fig. 3(b)]. We can explain this behavior theoretically by combining a simple model for a Weyl semimetal subject to a Zeeman field $\boldsymbol{B}(\boldsymbol{H}, T) = \mu_0[\boldsymbol{M}(\boldsymbol{H}, T) + \boldsymbol{H}]$. For $\boldsymbol{M}(\boldsymbol{H}, T)$ we take the behavior that follows from mean-field theory of a ferromagnet [see Fig. 3(d)]. Assuming that the main temperature dependence of the anomalous Hall conductivity stems from the temperature dependence of $\boldsymbol{M}(\boldsymbol{H}, T)$, we obtain the Hall conductivity by integration over the Berry curvature of occupied states. The result, shown in Fig. 3(c), reproduces the qualitative behavior of the experimental data above, at, and below T_C.

In summary, we studied the intrinsic AHE using the ferromagnetic Weyl semimetal PrAlGe as a case study. This AHE was derived from ZF extrapolation of the field-dependent Hall resistance. Consistent with previous results, finite values are observed below $T_C = 15$ K. Additionally, we present clear evidence that a similar extrapolated response is also found in the paramagnetic phase,

challenging the conventional understanding that such a response is synonymous with AHE and thereby a definitive indicator of TRSB. Muon spin relaxation measurements confirmed a paramagnetic phase above T_C without TRSB. Instead, by employing a mean-field theory approach, we explain the observed temperature dependence as a result from induced magnetization due to the applied magnetic field in the presence of strong ferromagnetic fluctuations. Our findings have profound implications for the study of AHE in systems where TRSB is contentious, such as kagome metals, potentially reshaping discourse in the field.

Acknowledgments—O. K. F. is supported by the Swedish Research Council (VR) via Grant No. 2022-06217 and the Foundation Blanceflor 2023 and 2024 fellow scholarships. X. L. acknowledges support from the National Key R&D Program of China (Grant No. 2022YFA1403700). M. H., K. K., Q. W., and J. C. acknowledge support from the Swiss National Science foundation (SNSF) under Grants No. 200021_188564 and No. BSSGI0_155873. Q. W. is supported by the Research Grants Council of Hong Kong (ECS No. 24306223). We acknowledge Diamond Light Source for time on Beamline I05 under Proposal SI22091. S. S. and T. S. acknowledge support from the SNSF under Grant No. 200021-188706. J. W. and V. U. acknowledge support from the SNSF Project No. 200021-188707 and Sinergia CRSII5-171003 NanoSkyrmionics. T. S. acknowledge the financial support from the National Natural Science Foundation of China (Grants No. 12374105 and No. 12350710785). Y. S. acknowledges funding from The Knut & Alice Wallenberg Fellow Grant No. 2021-0150 and the Swedish Research Council Dnr. 2017-05078. T. S. acknowledge the financial support from the National Natural Science Foundation of China (Grants No. 12374105 and No. 12350710785. The electrical resistivity and magnetization measurements were conducted at the Laboratory for Multiscale Materials Experiments at the Paul Scherrer Institute.

[1] M. Z. Hasan and C. L. Kane, Colloquium: Topological insulators, Rev. Mod. Phys. **82**, 3045 (2010).
[2] B. A. Bernevig, C. Felser, and H. Beidenkopf, Progress and prospects in magnetic topological materials, Nature (London) **603**, 41 (2022).
[3] Y. Machida, S. Nakatsuji, S. Onoda, T. Tayama, and T. Sakakibara, Time-reversal symmetry breaking and spontaneous Hall effect without magnetic dipole order, Nature (London) **463**, 210 (2010).
[4] S. Nakatsuji, N. Kiyohara, and T. Higo, Large anomalous Hall effect in a non-collinear antiferromagnet at room temperature, Nature (London) **527**, 212 (2015).
[5] J. Son, K.-H. Kim, Y. H. Ahn, H.-W. Lee, and J. Lee, Strain engineering of the Berry curvature dipole and valley magnetization in monolayer MoS_2, Phys. Rev. Lett. **123**, 036806 (2019).
[6] S.-C. Ho, C.-H. Chang, Y.-C. Hsieh, S.-T. Lo, B. Huang, T.-H.-Y. Vu, C. Ortix, and T.-M. Chen, Hall effects in artificially corrugated bilayer graphene without breaking time-reversal symmetry, National electronics review **4**, 116 (2021).
[7] N. Nagaosa, J. Sinova, S. Onoda, A. H. MacDonald, and N. P. Ong, Anomalous Hall effect, Rev. Mod. Phys. **82**, 1539 (2010).
[8] A. K. Nayak, J. E. Fischer, Y. Sun, B. Yan, J. Karel, A. C. Komarek, C. Shekhar, N. Kumar, W. Schnelle, J. Kübler, C. Felser, and S. S. P. Parkin, Large anomalous Hall effect driven by a nonvanishing Berry curvature in the noncolinear antiferromagnet Mn_3Ge, Sci. Adv. **2**, e1501870 (2016).
[9] T. Liang, J. Lin, Q. Gibson, S. Kushwaha, M. Liu, W. Wang, H. Xiong, J. A. Sobota, M. Hashimoto, P. S. Kirchmann, Z.-X. Shen, R. J. Cava, and N. P. Ong, Anomalous Hall effect in $ZrTe_5$, Nat. Phys. **14**, 451 (2018).
[10] S.-Y. Yang, Y. Wang, B. R. Ortiz, D. Liu, J. Gayles, E. Derunova, R. Gonzalez-Hernandez, L. Šmejkal, Y. Chen, S. S. P. Parkin, S. D. Wilson, E. S. Toberer, T. McQueen, and M. N. Ali, Giant, unconventional anomalous Hall effect in the metallic frustrated magnet candidate, KV_3Sb_5, Sci. Adv. **6**, eabb6003 (2020).
[11] C. Mielke, D. Das, J. X. Yin, H. Liu, R. Gupta, Y. X. Jiang, M. Medarde, X. Wu, H. C. Lei, J. Chang, P. Dai, Q. Si, H. Miao, R. Thomale, T. Neupert, Y. Shi, R. Khasanov, M. Z. Hasan, H. Luetkens, and Z. Guguchia, Time-reversal symmetry-breaking charge order in a kagome superconductor, Nature (London) **602**, 245 (2022).
[12] G. Zheng, C. Tan, Z. Chen, M. Wang, X. Zhu, S. Albarakati, M. Algarni, J. Partridge, L. Farrar, J. Zhou, W. Ning, M. Tian, M. S. Fuhrer, and L. Wang, Electrically controlled superconductor-to-failed insulator transition and giant anomalous Hall effect in kagome metal CsV_3Sb_5 nanoflakes, Nat. Commun. **14**, 678 (2023).
[13] H. Reichlova *et al.*, Observation of a spontaneous anomalous Hall response in the Mn_5Si_3 d-wave altermagnet candidate, Nat. Commun. **15**, 4961 (2024).
[14] X. Wei, C. Tian, H. Cui, Y. Zhai, Y. Li, S. Liu, Y. Song, Y. Feng, M. Huang, Z. Wang, Y. Liu, Q. Xiong, Y. Yao, X. C. Xie, and J.-H. Chen, Three-dimensional hidden phase probed by in-plane magnetotransport in kagome metal CsV_3Sb_5 thin flakes, Nat. Commun. **15**, 5038 (2024).
[15] G. Chang, B. Singh, S.-Y. Xu, G. Bian, S.-M. Huang, C.-H. Hsu, I. Belopolski, N. Alidoust, D. S. Sanchez, H. Zheng, H. Lu, X. Zhang, Y. Bian, T.-R. Chang, H.-T. Jeng, A. Bansil, H. Hsu, S. Jia, T. Neupert, H. Lin, and M. Z. Hasan, Magnetic and noncentrosymmetric weyl fermion semimetals in the ralge family of compounds (R = rare earth), Phys. Rev. B **97**, 041104(R) (2018).
[16] U. S. K. Paul C. Canfield, Tai Kong, and N. H. Jo, Use of frit-disc crucibles for routine and exploratory solution growth of single crystalline samples, Philos. Mag. **96**, 84 (2016).
[17] P. Puphal, C. Mielke, N. Kumar, Y. Soh, T. Shang, M. Medarde, J. S. White, and E. Pomjakushina, Bulk single-crystal growth of the theoretically predicted magnetic Weyl semimetals RAlGe (R = Pr, Ce), Phys. Rev. Mater. **3**, 024204 (2019).

[18] P. Puphal, S. Krebber, E. Suard, R. Cubitt, C. Wang, T. Shang, V. Ukleev, J. S. White, and E. Pomjakushina, Development of magnetism in the solid solution of $Ce_{1-x}Pr_xAlGe$: From magnetic topology to spin glass, Phys. Rev. B **101**, 214416 (2020).
[19] D. Destraz, L. Das, S. S. Tsirkin, Y. Xu, T. Neupert, J. Chang, A. Schilling, A. G. Grushin, J. Kohlbrecher, L. Keller, P. Puphal, E. Pomjakushina, and J. S. White, Magnetism and anomalous transport in the Weyl semimetal pralge: possible route to axial gauge fields, npj Quantum Mater. **5**, 5 (2020).
[20] D. S. Sanchez, G. Chang, I. Belopolski, H. Lu, J.-X. Yin, N. Alidoust, X. Xu, T. A. Cochran, X. Zhang, Y. Bian, S. S. Zhang, Y.-Y. Liu, J. Ma, G. Bian, H. Lin, S.-Y. Xu, S. Jia, and M. Z. Hasan, Observation of Weyl fermions in a magnetic non-centrosymmetric crystal, Nat. Commun. **11**, 3356 (2020).
[21] B. Meng, H. Wu, Y. Qiu, C. Wang, Y. Liu, Z. Xia, S. Yuan, H. Chang, and Z. Tian, Large anomalous Hall effect in ferromagnetic Weyl semimetal candidate pralge, APL Mater. **7**, 051110 (2019).
[22] J. M. Coey, *Magnetism and Magnetic Materials* (Cambridge University Press, Cambridge, England, 2010).
[23] A. Yaouanc and P. D. De Reotier, *Muon Spin Rotation, Relaxation, and Resonance: Applications to Condensed Matter* (Oxford University Press, New York, 2011), p. 147.
[24] O. K. Forslund, H. Ohta, K. Kamazawa, S. L. Stubbs, O. Ofer, M. Månsson, C. Michioka, K. Yoshimura, B. Hitti, D. Arseneau, G. D. Morris, E. J. Ansaldo, J. H. Brewer, and J. Sugiyama, Revisiting the *a*-type antiferromagnet $NaNiO_2$ with muon spin rotation measurements and density functional theory calculations, Phys. Rev. B **102**, 184412 (2020).
[25] O. K. Forslund, K. Papadopoulos, E. Nocerino, G. Morris, B. Hitti, D. Arseneau, V. Pomjakushin, N. Matsubara, J.-C. Orain, P. Svedlindh, D. Andreica, S. Jana, J. Sugiyama, M. Månsson, and Y. Sassa, Intertwined magnetic sublattices in the double perovskite compound $LaSrNiReO_6$, Phys. Rev. B **102**, 144409 (2020).
[26] N. Higa, T. U. Ito, M. Yogi, T. Hattori, H. Sakai, S. Kambe, Z. Guguchia, W. Higemoto, M. Nakashima, Y. Homma, A. Nakamura, F. Honda, Y. Shimizu, D. Aoki, M. Kakihana, M. Hedo, T. Nakama, Y.Ōnuki, and Y. Tokunaga, Critical slowing-down and field-dependent paramagnetic fluctuations in the skyrmion host euptsi: μSR and nmr studies, Phys. Rev. B **104**, 045145 (2021).
[27] See Supplemental Material at http://link.aps.org/supplemental/10.1103/PhysRevLett.134.126602 for additional information about the theoretical methods, which includes Refs. [28,29].
[28] S. Kourtis, J. Li, Z. Wang, A. Yazdani, and B. A. Bernevig, Universal signatures of Fermi arcs in quasiparticle interference on the surface of Weyl semimetals, Phys. Rev. B **93**, 041109(R) (2016).
[29] S.-B. Zhang, J. Erdmenger, and B. Trauzettel, Chirality Josephson current due to a novel quantum anomaly in inversion-asymmetric Weyl semimetals, Phys. Rev. Lett. **121**, 226604 (2018).
[30] Y. Deng, Y. Yu, M. Z. Shi, Z. Guo, Z. Xu, J. Wang, X. H. Chen, and Y. Zhang, Quantum anomalous Hall effect in intrinsic magnetic topological insulator $MnBi_2Te_4$, Science **367**, 895 (2020).
[31] A. Suter and B. M. Wojek, Musrfit: A free platform-independent framework for μSR data analysis, Phys. Procedia **30**, 69 (2012).
[32] O. K. Forslund, 1D to 3D magnetism in quantum materials: A study by muons, neutrons & x-rays, Ph.D. thesis, Kungliga tekniska högskolan, 2021.

End Matter

Appendix A: Electrical transport—A rectangular-shaped flux-grown PrAlGe single crystal was prepared for electrical transport. Four Au wires were attached to the *a*-*b* plane by silver paste to apply current (1 mA) and magnetic field along the crystallographic *a* and *c* axis, respectively, confirmed by x-ray Laue diffraction. Electrical resistivity (ρ_{xx}) and Hall resistivity (ρ_{xy}) were measured with both positive and negative fields to eliminate effects of contact misalignment. Figures 4(a) and 4(b) show magnetic field dependence of ρ_{xy} for selected temperatures. The intercept at ZF of the linear behavior extrapolated from higher fields defines ρ^A_{xy} and thereby $\sigma_{xy} = -\rho^A_{xy}/(\rho^2_{xx} + \rho^2_{xy})$.

Appendix B: Magnetic susceptibility—The temperature-dependent magnetic susceptibility of the flux-grown single-crystal PrAlGe was measured on the magnetic property measurement system (Quantum Design) equipped with the superconducting quantum interference device. The crystal was ZF cooled to base temperature, at which an excitation field of 1000 Oe was applied.

Appendix C: Angle resolved photo emission spectroscopy—Experiments were performed at the I05 beamline at Diamond Light Source above and below the FM ordering temperature $T_C = 15$ K. Floating-zone-grown PrAlGe crystals were cleaved *in situ* and measured in ultrahigh vacuum of $\sim 2 \times 10^{-10}$ mbar with a 50 μm beam spot. All presented spectra were collected with linear horizontal polarization on the (001) surface. Fermi level and spectral ARPES intensities were calibrated based on measurements from electrically contacted polycrystalline gold. To orient within the Brillouin zone, a photon energy ($h\nu$) scan was performed from 20 to 64 eV at $T = 10$ K. The out of plane Fermi surface along the (001) crystal axis, measured along the in-plane Γ-*M* direction is shown in Fig. 4(c). The photon energy was converted into k space via the relationship $k_z = (\sqrt{2m_e E_k(\cos^2\theta + V_0)}/\hbar)$, where m_e is the mass of the electron, E_k is the kinetic energy of emitted electron, θ is the emission angle, $\hbar$ is the reduced Planck constant, and $V_0 = 10$ eV is the inner potential. Each of the spectra have been

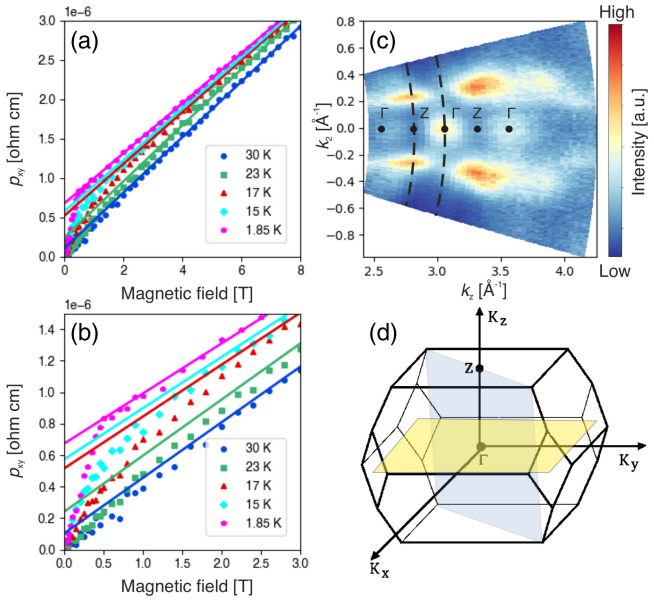

FIG. 4. (a), (b) Magnetic field dependence of the Hall resistivity (ρ_{xy}) for selected temperatures. The solid lines are linear fits between 2.5 and 8 T, extrapolated to ZF. (c) Out of plane Fermi surface along the (001) crystal axis, measured along the in-plane $\Gamma - M$ direction. We have defined $k_2 = k_x + k_y$ according to the main text. The dashed lines represent the Brillouin zone measured in this Letter. (d) Brillouin zone of PrAlGe [15]. Blue-shaded area highlights the scan direction of (c). The yellow-shaded area represents the Fermi surface presented in Figs. 1(a) and 1(b).

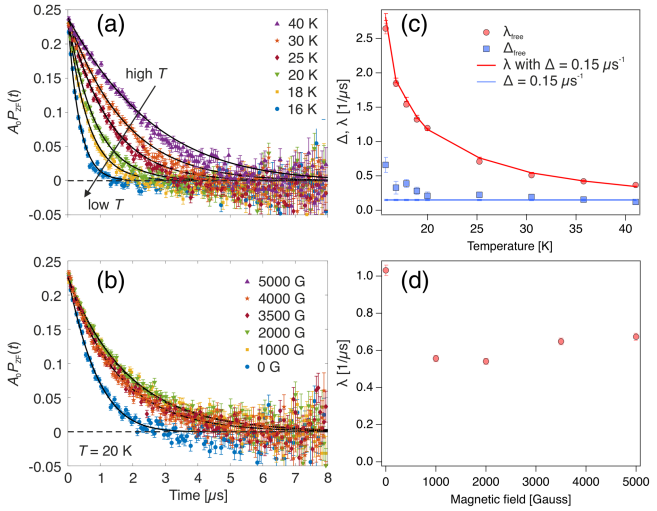

FIG. 5. (a), (b) Zero- and longitudinal-field muon spin relaxation time spectra. The solid lines represent best fits using Eq. (D1) with fixed $\Delta = 0.15\ \mu s^{-1}$. (c) λ and Δ as a function of temperature obtained through two different fitting procedures. The scattered points (λ_{free} and Δ_{free}) were obtained using a fit procedure with no restrictions made. The solid lines were obtained by fixing $\Delta = 0.15\ \mu s^{-1}$. (d) λ as a function of longitudinal fields, measured at $T = 20$ K.

normalized based on the total accumulated intensity. Figure 4(d) shows the Brillouin zone of PrAlGe [15], which highlights the relevant directions in this Letter.

Appendix D: Muon spin relaxation—The μ^+SR measurements were conducted on the GPS instrument at Paul Scherrer Institute. Muon spin relaxation time spectra were collected in ZF cooled configuration using a low background Cu fork holder inserted into a flow He cryostat reaching down to 1.6 K. Powdered polycrystalline ingots of PrAlGe were pressed into pellets of 5 mm in diameter. μ^+SR relies on implanting nearly 100% spin-polarized muons, acting as a local magnetometer. The high gyromagnetic ratio of the muon allows for measurements of weak (a few oersted) magnetic fields, sensitive to both static and dynamic magnetic field in the range of megahertz to gigahertz. The muon data were analyzed using MUSRFIT [31] and descriptions of the technique are found elsewhere [23,32].

Muon spin relaxation time spectra were collected as a function of temperature and LF. The measured ZF time spectra for selected temperatures are shown in Fig. 5(a). An exponential-like relaxation is presented for all $T > T_C = 15$ K. Therefore, the time spectra were fitted using an exponentially relaxing longitudinal field static Gaussian Kubo-Toyabe function

$$A_0 P_{\mathrm{ZFLF}}(t) = A G^{\mathrm{LFSGKT}}(\Delta, t, B_{\mathrm{LF}}) e^{-\lambda t}, \qquad \text{(D1)}$$

where A_0 is the initial asymmetry, a value determined by the instrument, and P_{ZFLF} is the muon spin relaxation function under LF and ZF (with $B_{\mathrm{LF}} = 0$ G). G^{LFSGKT} represents the longitudinal field static Gaussian Kubo-Toyabe function, where Δ is the field distributing width and λ is the exponential relaxation rate. Setting $B_{\mathrm{LF}} = 0$ G reduces G^{LFSGKT} into the static Gaussian Kubo-Toyabe (G^{SGKT}) function. The response of a muon ensemble originating from two independent magnetic field distributions is given by the Fourier transform of their convolution. Therefore, the total response can be modeled as a product of each response. In this case, the exponential relaxation entails fluctuating electronic moments, whereas G^{SGKT} represents field distributions arising from mostly $I_{\mathrm{Pr}} = 5/2$ and $I_{\mathrm{Al}} = 5/2$ randomly oriented nuclear moments.

Figure 5(c) shows λ and Δ as a function of temperature obtained in ZF through two different fitting procedures. λ_{free} and Δ_{free} were obtained using a fit procedure with no restrictions made. In this case, Δ_{free} increases as λ_{free} increases at lower temperatures. This kind of behavior is, however, nonphysical, assuming that there is no coupling between nuclear and electronic moments. Instead, this increase is a fitting artifact where the value of Δ_{free} is obscured by λ_{free}, as λ_{free} increases to very high values ($> 1\ \mu s^{-1}$). In fact, a single exponential can fit the ZF spectra at lower temperatures < 20 K and the Kubo-Toyabe component is not needed to reproduce the spectra. Although, a nuclear depolarization is, in principle, always there and

including the Kubo-Toyabe relaxation represents a more correct physical description.

To account for the described fitting defect, a proper value of Δ needs to be estimated. The relaxation rate (λ) decreases with increasing temperature. Therefore, all ZF time spectra collected at temperatures above 20 K were simultaneously fitted with having Δ as a shared parameter, in which $\Delta \simeq 15\ \mu s^{-1}$ was obtained. The presented λ in Fig. 2(d) is the obtained temperature dependence with $\Delta = 15\ \mu s^{-1}$ fixed. It is noted that, regardless of the fitting procedure, very similar temperature dependencies are obtained for the exponential relaxation rate [Fig. 5(c)].

Figures 5(b) and 5(d) show measured muon spin time spectra and the corresponding relaxation rate (λ) as a function of LF collected at $T = 20$ K. All time spectra were fitted simultaneously by having $\Delta = 0.15\ \mu s^{-1}$ and the asymmetry (A) as a shared parameter, effectively reducing the number of fit parameters to one (λ). Apart from the initial decoupling (the decrease in λ), there is no significant LF dependence observed. The initial decrease in relaxation rate can be mostly attributed to nuclear moments, though a small fraction of static or slowly fluctuating fields may be present as well. However, no further decrease is observed beyond the initial decoupling, indicating that the dominant fluctuations persist up to at least 5000 G.

Below T_C, the time spectra exhibit a rapid relaxation followed by a slow relaxation [Fig. 2(c)]. In a perfect powder, $2/3$ of the internal magnetic field is expected to be perpendicular and $1/3$ of the internal magnetic field is expected to be parallel with respect to the initial muon spin polarization. However, the time spectra below T_C do not exhibit this ratio between the parallel and perpendicular components. This is because the polycrystals used in this Letter exhibits a preferred orientation. The tetragonal crystals have a strong c-axis preference, which is the FM order direction. This causes a higher asymmetry (signal) in the parallel component compared to the perpendicular one.